



Sand mineralogy, origin, uniformity and weathering ratio of some soils in El-Galaba plain, Aswan, Egypt

Zidan M. A. M.^{*}, Faragallah M. A., El-Desoky A. I., Sayed Y. A.

Department of Soils and Water, Faculty of Agriculture, Al-Azhar University, Assiut 71524, Egypt

Abstract

The main aims of this study are to study the mineralogical composition of very fine sand fraction and estimating the origin, uniformity and weathering degree of the soil material in the soils of the investigated area. A total of forty-three soil samples were collected from twelve soil profiles according to the pedomorphologic variations. The investigated soil profiles show a coarse texture of sand and loamy sand, as well as moderately coarse texture of sandy loam. The light fraction was the fundamental constituent of the very fine sand fraction of the studied soils. Furthermore, all soil samples of the studied area were exhibits relatively low contents of heavy fraction in the very fine sand fraction and their index figures. The light minerals were mainly composed of quartz followed by feldspars, with irregular distribution of these minerals with depth. Opaques minerals were the most predominant constituent in all samples. They range from 35.78 to 91.25 % of the heavy fraction, without any systematic vertical distribution. Whereas the non-opaques were the less abundant in the heavy minerals of most of the studied soil samples and include zircon, tourmaline, pyroxenes (augite and enstatite), garnet, epidot, rutile, biotite, amphiboles (hornblende) and staurolite. The assemblages and frequencies of these light and heavy minerals of the studied soil samples suggest that the origin of these soils derived from different provenances. Regarding, uniformity of the studied profiles, the results showed these soils were formed from materials of heterogeneity nature and could be considered young from the pedologic point of view. These results also showed that weathering ratios in the surface layer were lower than in the subsurface layer of the majority of soil profiles reflecting a slight effect of weathering in the surface layer and pronounced amounts of the resistance minerals in these sediments.

Keywords: sand mineralogy, soil origin, uniformity, weathering, El-Galaba plain.

*Corresponding author: Zidan M. A. M.,
E-mail address: zedanaswan@gmail.com

1. Introduction

The variations in soil properties are usually attributed to the changes in climate, soil runoff, erosion, and sedimentation processes which affect soil origin and uniformity (Sulieman *et al.*, 2021). Studying of heavy minerals is considered as criteria for establishing genesis and uniformity of soil parent material. The study of parent material uniformity is a very vital and suitable media for assessing pedological processes and forming the soils (Lizzoli *et al.*, 2021). The resistant heavy minerals and their distributions vertically within the upper horizons of solum have been utilized to distinguish between pedological and geological processes (Siqueira *et al.*, 2021). Varied species of heavy minerals have been employed but the most common minerals in dry soils are quartz, xenotime, zircon, tourmaline, and rutile (Salman *et al.*, 2021). Numerous mineralogical studies have been carried out on the Egyptian Desert soils by Faragallah and Essa (2011), Amer *et al.* (2020), Elwan (2021), Aref *et al.* (2021) and Yossif *et al.* (2022). Mineralogical studies are usually carried out on the fine and very fine sand sub fractions to know the type and distribution of constituent minerals in soils and rocks. Studies on heavy minerals have been used by soil scientists to answer the questions of the origin of soil material and to recognize the depositional differences in horizons of soil profiles as well as an index of

weathering processes throughout the soil profile, an indicator of the level of most plant nutrients, and a base for evaluating profile soil development (Amer *et al.*, 2020; Yossif *et al.*, 2022). Faragallah and Essa (2011) studied that the mineralogical composition of khamasin wind dust between the fringes of eastern and western deserts throughout the Nile valley, Assiut. They found the minerals of the khamasin dust in 2008 were in the order of quartz> K-feldspar> calcite> magnetite> epidote> anhydrite> garnet> augite> tourmaline> zircon> limenite> plagioclase>goethite> actinolite> hematite. However, the minerals of the khamasin dust in 2009 had the order of quartz> K-feldspar> calcite> epidote> magnetite> tourmaline> anhydrite> augite> plagioclase> limenite> rutile> hematite>limonite> hematite> garnet> actinolite. Mineralogical composition of the sand fraction in some soils of south Tushka area showed that light minerals were the major component and mainly dominated by quartz which constitutes more than 89%. Feldspars are depicted with a few amounts not exceed 11% and represented by plagioclase, orthoclase and microcline. On the other hand, heavy minerals were the least and dominated by opaques which constitute from 33% to 60.3%. Non-opaque minerals were dominated by pyroboles (pyroxene + Amphiboles) followed by very stable minerals (Zircon, rutile and tourmaline). Slightly stable minerals (garnet and epidote) and stable minerals (staurolite, kyanite, silimanite and andalusite) are

found in less pronounced amounts (Amer *et al.*, 2020). Elwan (2021) studied some soils in west El-Minia, Western Desert, Egypt and he found that the light minerals associations in the studied soils were dominated by quartz, gypsum, feldspars, calcite, mica, and chlorite. However, heavy mineral percentages (1.46 – 16.34%) were increased from the west to the east of the investigated transect across the slope gradient. The highest concentration of heavy minerals (10.09 – 16.34%) was detected in the lower soils. The identified heavy minerals were pyroxene (augite and hyperthene), amphiboles (hornblende and actinolite), garnet, staurolite, kyanite, zircon, tourmaline, rutile, epidote, zoisite, biotite, monazite, glauconite, and opaques. Opaque minerals (39.33 to 61.33%) constitute the most predominant constituent in all studied soil samples. The heavy minerals characteristics suggest their mixed sources from sandstone, limestone, and metamorphic rocks. Some soils of west Manfalut, Assuit, Egypt have highest frequency of opaques and ubiquitous was found in the

north of the study area. Furthermore, pyroboles and para-metamorphic minerals were detected in maximum contents in the south portion. A significant positively correlation was found between Augite & Apatite, while a significant negatively one was observed between Tourmaline and Zircon. Maturity index values were dominantly less than 75%, indicating weakly developed soils. Morphological characterization and vertical distribution of Z/T, Z/R, and Z/R+T showed that parent materials of the investigated soils are apparently formed of heterogeneous depositional regimes (Aref *et al.*, 2021).

2. Materials and methods

2.1 Site description

The investigated area is located at the western part of the Nile Valley of Egypt, approximately 35 km northwest Aswan in the western desert. It lies between longitudes 32°35'00" and 32°48'00"E and latitudes 24°35'00" and 24°45'00"N (Figure 1).

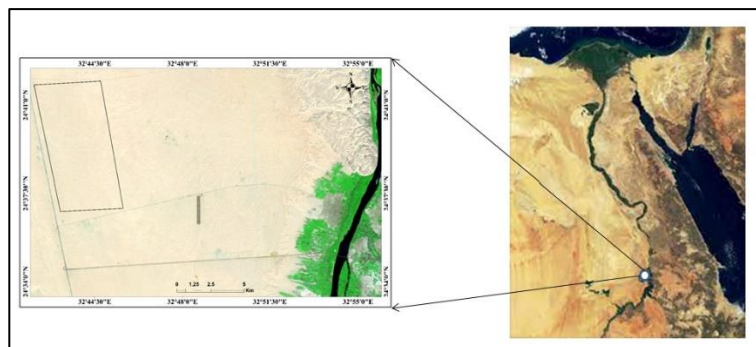


Figure (1): A location map of the study area.

The study area is a desert region with no land use. According to Saleh *et al.* (2015) the climatic conditions of El-Galaba plain region are typically a desert like condition characterized by an extremely arid climate with long hot rainless summer, mild winter with very low to no amount of rainfall. The mean temperature in winter ranges from 16.1 to 18.7 °C and 15.9 to 17.3 °C in Aswan and Kom Ombo stations, respectively. In summer, the mean temperature ranges from 32.9 °C to 33.4 °C and 32.4 to 33 °C in Aswan and Kom Ombo stations, respectively. The intensity of rainfall at El-Galaba area is very low to negligible as the annual intensity reaches 0.7 mm in Aswan and 1.2 mm in Kom Ombo stations, respectively, while no rain is recorded in summer. Although rainfall is not significant throughout the year, some rare and irregular storms take place over scattered localities during the winter season. El-Galaba plain area represents a part of the geological formation of the western desert as illustrated in Figure (2) and it can be summarized as follows:

1) Umm Barmil Formation (Santonian-Campanian) is exposed to the south and southwest of the investigated region and it forms low topographic hills. It is composed of fluvial sandstone sequences with cross-bedded sandstone.

2) Quseir Formation (Campanian) crops out to the east which is close to the River Nile in the north at Faris village. It is made of fine sandstone and siltstone

beds.

3) Duwi Formation (Campanian) crops out as relic hills in the west of Idfu. It consists of Phosphate beds and glauconitic sandstone (Said, 1990).

4) Dakhal Formation (Maastrichtian–Paleocene) is well exposed in G. El Borga and Sinn El Kaddab plateau with a thickness of 131 m. It consists mainly of dark gray marine shale with calcareous intercalations (Hewaidy and Soliman, 1993).

5) Kurkur Formation (Paleocene), which is exposed in the scarp face of the Sinn El Kaddab plateau, directly overlies Dakhla Formation and underlies Garra Formation. It consists of phosphatic limestone with silty shale and marl intercalations that have thickness of 21 m (Ali, 2003).

6) Garra Formation (Paleocene) is well exposed in the G. El Boraga and the scarp face of Sinn El Kaddab plateau with a thickness of 30 m of grayish white limestone and marl beds (Ali, 2003). A lower Eocene crops out in Sinn El Kaddab plateau and comprises Dungul, (brown reefal limestone), El-Rufuf (well bedded limestone) and Serai Formations (thinly bedded limestone). Quaternary deposits cover areas in the west of Idfu-KomOmbo. These are described as sand, sandy gravels and gravels from some of the distributed quarrying in the west of Idfu and Faris village (Basheer and Mosaad, 2018).

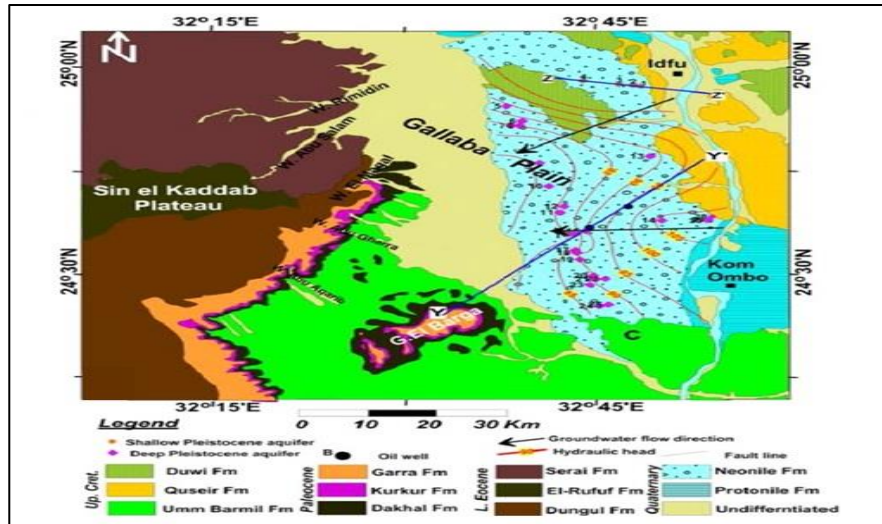


Figure (2): Geological map of El-Galaba plain region modified from Conoco (1987) (adopted from Mosaad and Basheer, 2020).

2.2 Remote Sensing and GIS works

In the current study, remote sensing tool was used, and it was expressed by Landsat 8 operational land imager (OLI) satellite image dated 2018/03/28, in row 43 and path 174 (Figure 3). The bands were chosen with the ultimate applications of the data more firmly in mind. A selection of the most adequate combination of bands (7, 5, and 3) was executed in this study according to NASA (2013). The image has a swath width of 170 km × 185 km with a spatial resolution of 30 m. In the current study, remote sensing tool was used, and it was expressed by Landsat 8 operational land imager (OLI) satellite image dated 2018/03/28, in row 43 and path 174 (Figure 3). The bands were chosen with the ultimate applications of the data more firmly in mind. A selection of the most

adequate combination of bands (7, 5, and 3) was executed in this study according to NASA (2013). The image has a swath width of 170 km × 185 km with a spatial resolution of 30 m. The images were geometrically corrected, and rectification method was followed. The geometric model used in the rectification process was second order polynomial and the resampling method is the nearest neighbour method. Digital Elevation Model (DEM) was used as the source data for elevation heights of the study area (Figure 4). Geographic information systems (GIS) works including base map, digital elevation model (DEM) and distribution of heavy minerals of the sand fraction in the soil surface layers maps were produced using ArcGIS 10.4.1 software (ESRI, 2014). Map production for presentation or visual analysis and interpretation includes pixel, map and

geographic (latitude/longitude) grids; polygons, polylines and geometric shapes; scale-bars; north arrows; text and symbols; map keys, legends and image insets.

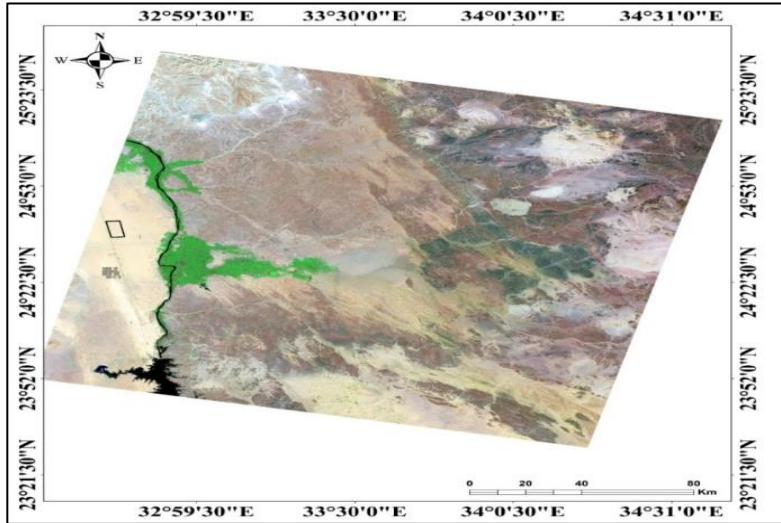


Figure (3): Landsat 8 operational land imager (OLI) satellite image.

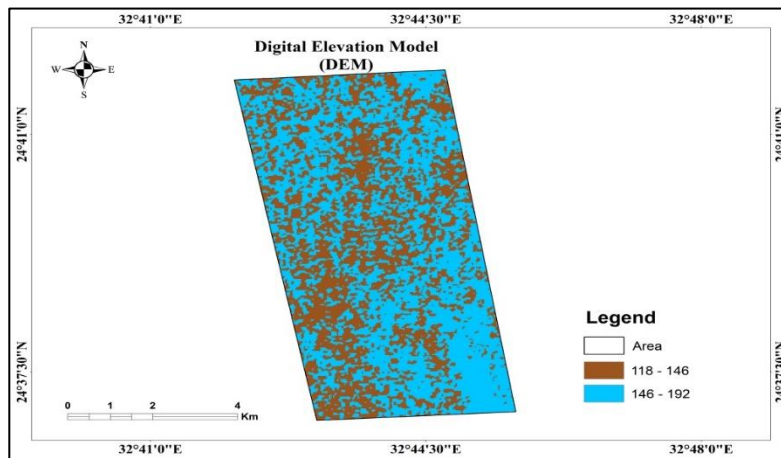


Figure (4): Digital elevation model of the study area.

2.3 Field studies

A semi-detailed survey was conducted in the study area; thus, thirty-six soil

profiles were dug down to the suitable depth according to the nature of the soil material unless it was hindered by a bed rock or water table. The locations of

these soil profiles were recorded in the field using the Global Positioning System "Garmin GPS" as given in Figure (5). Sixty-seven representative soil samples were collected from different layers of all investigated soil profiles according to the

pedomorph variations. The mechanical analysis of each layer was carried out. According to the soil texture of layers twelve soil profiles were selected to study of mineralogical composition of sand fraction (Figure 6).

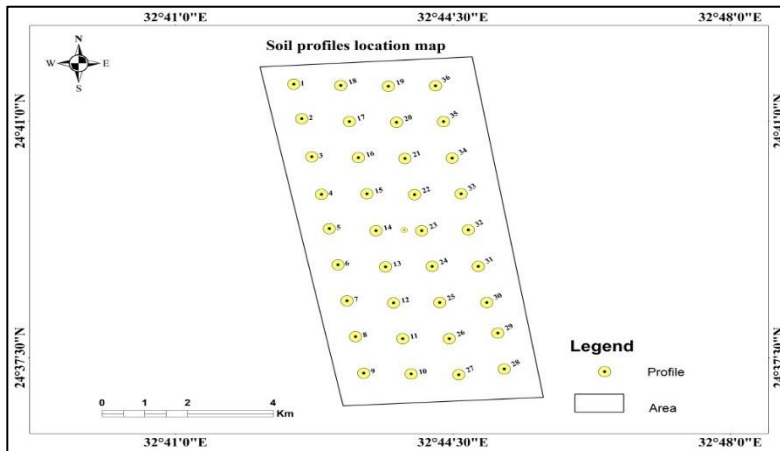


Figure (5): A soil profiles location map.

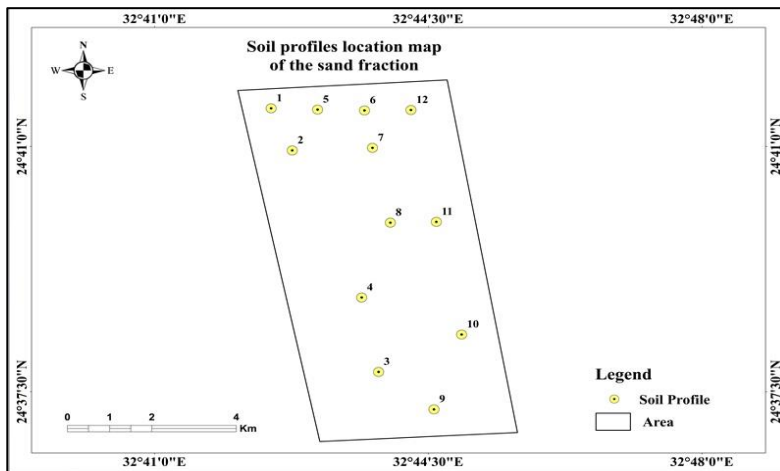


Figure (6): soil profiles location map of the sand fraction.

2.4 Analytical methods

The collected soil samples were air-dried,

crushed, sieved to pass through 2 mm sieve and stored in plastic containers for different analysis. The physical

properties and mineralogical analyses of the investigated soil samples were determined at Faculty of Agriculture laboratories, Al-Azhar University, Assuit Egypt.

2.4.1 Some physical properties

The gravel content was measured by volume according to Schoenberger *et al.* (2012). The particle-size distribution of the soil samples was performed using the pipette method that was described by Gavlak *et al.* (2005).

2.4.2 Mineralogical analysis of the sand fraction

Forty-three soil samples from twelve soil profiles of the investigated area were prepared for the examination of light and heavy minerals using Brewer (1964) method. Accordingly, soil samples were treated with sodium acetate (Na C₂H₃O₂.3H₂O) 0.5 M, 136 g/l, adjusted to pH 5 with acetic acid for carbonate removal, 30% H₂O₂ for organic matter and manganese oxides removal. The soil samples were washed with distilled water to ensure the removal of soluble salts. After decantation of both silt and clay, the sand fractions (63-125 μ) were separated, then washed, dried and kept for minerals examination. The separated sand fraction was re-sieved through a 100 μm sieve to obtain the very fine sand (50-100 μm). Separation of heavy and light minerals in the very fine sand was carried out using bromoform separation

(sp.g. 2.85) technique. Mounting of heavy and light fractions was undertaken according to the method described by Brewer (1964), in which the grains were first fixed to slides with natural Canada balsam (R.I = 1.538). The index figure was calculated as follows:

$$\text{Index figure} = \frac{\text{Heavy mineral weighted}}{\text{Light mineral weighted}} \times 100$$

About 500 mineral grains were identified and counted in each slide using the polarizing microscope. The minerals described and identified according to Kerr (1959) and Milner (1962). The ratios between two or more of the highly resistant minerals were used to evaluate the soil uniformity and maturity, while the ratios between the less stable and ultra stable minerals were used to evaluate the weathering rate and the development of soils according to Brewer (1964) and Hammad (1968).

2.4.3 Calculation of uniformity and weathering ratios

According to Chapman and Horn (1968) the uniformity ratios were applied as zircon / tourmaline (Z/T), zircon /rutile (Z/R) and zircon / (rutile + tourmaline) (Z/R+T) for different layers of soil profile. Concerning weathering rate, the ratios between the most susceptible weathered minerals (amphiboles and pyroxenes) and the more resistance ones (zircon and tourmaline) as formula of A+P / Zr+T and H / Zr+T are calculated

for the assessment of the efficiency of weathering processes throughout the studied soil profiles.

3. Results and discussion

3.1 Particle-size distribution

Nearly every of the soil use and management is influenced by soil texture, which refers to the proportions of sand, silt and clay. It plays a key role in controlling a variety of physical and chemical properties of soil, especially when fine particles found more prevalent (Poeplau and Kätterer, 2017). Data in Table 1 reveal that, the investigated soil profiles show a coarse texture of sand and loamy sand, as well as moderately coarse texture of sandy loam according to Sys (1979). These respective texture grades represent 79.07, 18.60 and 2.33%, respectively, of the soil samples in this investigated area. Additionally, the studied soil samples have 91.54, 4.19% and 4.27% as average contents of sand, silt and clay, respectively (Table 1). Different layers of most soil profiles exhibit no systematic pattern of sand, silt and clay contents with depth. The average of gravel content is 15.09% without any specific trend of their distribution with depth. Most of soil samples in the study area have gravels

content less than 15%.

3.2 Mineralogy of the sand fraction

Minerals in the sand fraction are inherited from the parent material or formed during alteration. The kind and amount of heavy minerals present in the soil are associated to its origin and that semiquantitative determination of such minerals are usually adequate to establish soil origin.

3.2.1 Light minerals

The main dominant minerals in the investigated portion are quartz followed by feldspars. Quartz grains are colourless of low relief and occur mainly as single irregular grains. The dominance of quartz over other members of the light minerals is mostly related to its resistance to weathering and disintegration during the multi cyclic processes of sedimentation. Other light minerals are plagioclase, orthoclase and microcline. Their grains are usually colourless, low relief, having distinct cleavage and showing twinning property. In soils feldspars are usually cloudy and slightly weathered whereas quartz is usually clear. On the other hand, the presence of feldspars could be taken as indication for the weathering prevailed during the soil formation that was not so drastic to cause a complete dissolution of minerals susceptible to weathering.

Table (1): Some Physical properties of the soil profiles of the studied area.

Profile No.	Depth (cm)	Sample No.	Gravel by volume (%)	Particle-size distribution			
				Sand (%)	Silt (%)	Clay (%)	Texture grade
1	0 - 20	1	3.87	88.87	6.38	4.75	Sand
	20 - 60	2	25.34	96.87	1.87	1.26	Gravelly sand
	60 - 70	3	22.27	97.67	1.55	0.78	Gravelly sand
	70 - 150	4	8.99	98.47	0.74	0.79	Sand
2	0 - 25	5	4.81	94.47	2.96	2.57	Sand
	25 - 50	6	25.51	95.27	3.15	1.58	Gravelly sand
	50 - 110	7	8.24	96.07	1.55	2.38	Sand
	110 - 120	8	28.81	96.87	1.72	1.41	Gravelly sand
	120 - 150	9	13.07	94.47	2.87	2.66	Sand
3	0 - 25	10	4.27	91.27	3.47	5.26	Sand
	25 - 45	11	5.65	89.75	3.87	6.38	Sand
	45 - 55	12	27.41	88.07	5.55	6.38	Gravelly loamy sand
	55 - 120	13	18.39	89.67	4.75	5.58	Gravelly sand
	120 - 150	14	25.19	89.67	4.75	5.58	Gravelly sand
4	0 - 35	15	2.02	93.67	1.95	4.38	Sand
	35 - 70	16	17.91	91.27	3.56	5.17	Gravelly sand
	70 - 110	17	18.13	96.07	0.75	3.18	Gravelly sand
	110 - 150	18	13.82	96.87	0.83	2.30	Sand
5	0 - 30	19	2.60	95.27	3.15	1.58	Sand
	30 - 60	20	4.28	92.87	3.17	3.96	Sand
	60 - 80	21	22.20	85.87	7.59	6.54	Gravelly loamy sand
	80 - 105	22	28.97	92.07	4.08	3.85	Gravelly sand
	105 - 150	23	19.66	92.07	3.95	3.98	Gravelly sand
6	0 - 20	24	1.39	97.67	0.75	1.58	Sand
	20 - 40	25	9.66	89.67	6.35	3.98	Sand
	40 - 150	26	20.58	77.14	13.37	9.49	Gravelly sandy loam
7	0 - 20	27	1.41	97.67	0.85	1.48	Sand
	20 - 45	28	28.88	85.95	7.67	6.38	Gravelly loamy sand
	45 - 150	29	19.67	93.67	2.35	3.98	Gravelly sand
8	0 - 25	30	1.28	91.48	3.74	4.78	Sand
	25 - 65	31	4.44	93.89	2.94	3.17	Sand
	65 - 90	32	21.67	90.47	4.75	4.78	Gravelly sand
9	90 - 150	33	18.81	90.47	4.26	5.27	Gravelly sand
	0 - 20	34	5.67	80.93	10.30	8.77	Loamy sand
	20 - 55	35	22.24	85.67	8.97	5.36	Gravelly loamy sand
	55 - 150	36	21.31	90.47	4.75	4.78	Gravelly sand
10	0 - 50	37	3.61	93.67	0.89	5.44	Sand
	50 - 150	38	27.06	86.67	6.95	6.38	Gravelly loamy sand
11	0 - 20	39	9.65	90.14	3.89	5.97	Sand
	20 - 80	40	28.14	84.10	8.80	7.10	Gravelly loamy sand
	80 - 150	41	17.29	96.07	0.75	3.18	Gravelly sand
12	0 - 25	42	6.63	83.32	9.60	7.08	Loamy sand
	25 - 150	43	28.18	93.67	3.95	2.38	Gravelly sand
Minimum			1.28	77.14	0.74	0.78	-----
Maximum			28.97	98.47	13.37	9.49	-----

The frequency distribution of light minerals of the sand fraction in the studied soil profiles is present in Table (2). The data manifest that quartz is the most abundant mineral in all the estimated samples. Quartz frequency differs between 98.18 and 99.78% of the light fraction. While feldspars comprise

up to 1.82% as a maximum content of the light fraction. The fundamental constituent of feldspars is plagioclase, meanwhile orthoclase and microcline are present as lower contents or traces. Both quartz and feldspars minerals are not easily impacted by weathering processes, therefore their distribution could serve as

an indication of uniformity of parent materials.

Table (2): Frequency distribution of the light minerals in the sand fraction (63-125 μ) of the representative soil profiles.

Profile No.	Depth (cm)	Quartz (%)	Feldspars (%)		
			Plagioclase	Orthoclase	Microcline
1	0 - 20	98.54	0.76	0.49	0.21
	20 - 60	99.71	0.16	0.10	0.03
	60 - 70	98.57	0.63	0.48	0.32
	70 - 150	98.83	0.47	0.47	0.23
2	0 - 25	99.78	0.12	0.03	0.06
	25 - 50	99.78	0.16	0.05	0.00
	50 - 110	99.38	0.36	0.13	0.13
	110 - 120	99.13	0.32	0.39	0.16
	120 - 150	99.57	0.36	0.00	0.06
3	0 - 25	99.65	0.19	0.08	0.08
	25 - 45	99.43	0.25	0.11	0.22
	45 - 55	99.44	0.36	0.10	0.10
	55 - 120	99.74	0.17	0.05	0.05
	120 - 150	99.45	0.38	0.04	0.13
4	0 - 35	99.51	0.28	0.09	0.11
	35 - 70	99.49	0.19	0.13	0.19
	70 - 110	98.18	0.91	0.51	0.41
	110 - 150	98.68	0.80	0.17	0.34
5	0 - 30	99.15	0.37	0.31	0.18
	30 - 60	99.56	0.19	0.12	0.12
	60 - 80	99.04	0.36	0.16	0.44
	80 - 105	98.99	0.62	0.22	0.17
	105 - 150	98.82	0.51	0.26	0.41
6	0 - 20	99.36	0.25	0.22	0.16
	20 - 40	99.73	0.14	0.07	0.07
	40 - 150	99.55	0.22	0.22	0.00
7	0 - 20	99.25	0.42	0.23	0.09
	20 - 45	99.37	0.28	0.14	0.21
	45 - 150	98.63	0.50	0.32	0.55
8	0 - 25	99.62	0.20	0.03	0.14
	25 - 65	99.39	0.36	0.05	0.20
	65 - 90	99.15	0.49	0.22	0.13
	90 - 150	99.55	0.06	0.17	0.23
9	0 - 20	99.66	0.12	0.18	0.03
	20 - 55	99.35	0.32	0.08	0.24
	55 - 150	99.39	0.31	0.06	0.25
10	0 - 50	99.61	0.16	0.07	0.16
	50 - 150	99.75	0.08	0.04	0.12
11	0 - 20	99.39	0.26	0.21	0.14
	20 - 80	99.39	0.24	0.09	0.28
	80 - 150	98.70	0.52	0.26	0.52
12	0 - 25	98.95	0.46	0.35	0.25
	25 - 150	98.70	0.62	0.28	0.40
Minimum		98.18	0.06	0.00	0.00
Maximum		99.78	0.91	0.51	0.55

3.2.2 Heavy minerals

The main heavy minerals which were detected in the studied samples are opaques, zircon, tourmaline, pyroxenes

(augite and enstatite), garnet, epidot, rutile, biotite, amphiboles (hornblende) and staurolite. The frequency distribution of the heavy minerals could be discussed in the same order as given in Table (3).

Table (3): Frequency distribution of heavy minerals of the studied soil profiles.

Profile No.	Depth (cm)	Opaques	Zircon	Tourmalin	Pyroxenes		Garnet	Epidot	Rutile	Biotite	Amphiboles Hornblend	Staurolite
					Augit	Enstatite						
1	0 - 20	63.75	22.50	6.60	1.91	1.04	1.10	0.52	0.93	0.70	0.49	0.46
	20 - 60	77.12	7.30	4.10	3.62	1.55	0.80	2.07	1.55	0.40	1.03	0.37
	60 - 70	57.58	14.10	3.00	7.07	10.10	1.00	4.04	1.01	1.00	1.01	0.00
	70 - 150	35.78	18.30	5.50	11.01	7.34	6.40	4.59	3.67	4.60	1.83	0.92
2	0 - 25	60.21	13.70	8.00	3.85	1.03	3.10	2.76	2.89	1.80	1.28	1.48
	25 - 50	62.22	18.70	4.90	4.89	1.11	1.10	1.11	2.22	2.20	0.89	0.67
	50 - 110	81.17	4.00	2.80	2.77	1.50	1.10	2.17	0.84	2.50	0.84	0.30
	110 - 120	54.25	13.10	3.90	7.19	3.27	2.00	5.88	2.61	3.90	2.61	1.31
	120 - 150	62.60	15.20	3.50	3.52	1.63	1.10	2.98	1.90	4.60	1.90	1.08
3	0 - 25	61.13	20.90	7.80	2.19	0.55	1.60	2.28	1.37	0.80	1.00	0.46
	25 - 45	63.19	18.00	7.60	1.99	0.40	2.90	0.88	2.55	0.60	0.96	0.88
	45 - 55	77.49	14.70	3.10	0.51	0.20	0.90	0.42	1.44	0.60	0.44	0.15
	55 - 120	79.21	10.40	3.10	1.30	0.45	1.60	0.39	1.04	1.90	0.26	0.32
	120 - 150	75.80	11.50	4.70	2.14	0.59	1.10	0.36	1.07	1.80	0.47	0.47
4	0 - 35	69.28	15.60	9.20	1.51	0.47	0.90	0.61	1.04	0.60	0.68	0.18
	35 - 70	75.79	13.00	4.10	1.58	0.34	0.70	0.57	2.26	0.90	0.57	0.23
	70 - 110	79.12	9.80	2.90	1.25	0.63	1.50	1.04	1.67	1.30	0.63	0.21
	110 - 150	75.57	8.50	5.00	3.45	2.16	1.10	1.29	0.72	0.90	1.15	0.14
5	0 - 30	68.73	12.80	10.50	1.10	1.22	1.20	1.22	0.99	0.90	0.88	0.44
	30 - 60	66.63	13.70	11.00	1.87	0.41	1.30	1.32	0.56	1.30	1.37	0.46
	60 - 80	74.53	14.20	3.90	1.68	0.84	0.60	1.05	1.68	0.80	0.52	0.21
	80 - 105	77.49	9.20	7.00	1.43	0.86	0.80	0.62	0.72	0.90	0.81	0.33
	105 - 150	74.64	9.00	6.90	2.59	2.13	0.60	0.69	0.91	1.40	0.84	0.38
6	0 - 20	59.01	9.50	8.10	8.11	4.05	1.80	2.25	1.80	3.20	1.35	0.90
	20 - 40	76.46	10.40	6.30	1.77	0.67	0.50	0.53	1.73	0.60	0.62	0.38
	40 - 150	83.68	7.90	1.60	1.17	0.42	0.70	0.84	2.43	0.30	0.42	0.59
7	0 - 20	75.77	5.50	11.60	1.38	0.79	0.30	0.40	1.09	0.50	2.18	0.49
	20 - 45	75.63	8.20	6.70	2.65	1.53	1.00	0.84	1.11	0.30	1.25	0.84
	45 - 150	86.71	4.40	2.80	1.28	0.78	0.30	0.46	1.24	1.30	0.46	0.23
8	0 - 25	80.12	6.00	7.70	1.02	0.68	0.50	1.57	0.88	0.30	1.02	0.27
	25 - 65	82.44	5.70	5.90	1.57	0.59	0.40	0.65	0.59	1.30	0.59	0.27
	65 - 90	82.39	6.30	5.60	0.74	1.05	0.30	0.84	0.91	0.60	0.98	0.35
	90 - 150	86.71	3.20	3.20	1.49	1.06	0.60	0.91	0.91	0.60	1.20	0.14
9	0 - 20	80.21	8.80	5.50	0.91	0.33	0.70	1.00	1.29	0.40	0.48	0.33
	20 - 55	83.36	6.80	1.90	2.02	0.62	1.10	1.24	1.09	0.50	0.93	0.47
	55 - 150	88.05	3.50	3.00	1.11	0.32	0.60	0.65	0.46	1.60	0.42	0.42
10	0 - 50	78.50	3.60	10.60	1.06	0.69	1.40	0.98	0.69	0.50	1.14	0.74
	50 - 150	91.25	2.20	1.70	1.03	0.57	0.70	0.69	0.40	0.70	0.40	0.40
11	0 - 20	87.00	2.70	4.90	0.94	0.36	0.60	0.50	1.20	0.60	0.86	0.34
	20 - 80	85.07	4.50	2.00	1.77	0.55	1.10	0.77	2.21	1.10	0.22	0.66
	80 - 150	80.14	3.50	2.10	2.84	1.42	0.70	0.71	2.13	2.80	1.42	2.13
12	0 - 25	81.76	4.20	5.90	1.28	0.90	1.10	0.54	1.70	0.60	1.25	0.71
	25 - 150	87.86	2.10	1.10	2.97	2.24	0.90	0.33	0.94	0.70	0.57	0.33
Minimum		35.78	2.10	1.10	0.51	0.20	0.30	0.33	0.40	0.30	0.22	0.00
Maximum		91.25	22.50	11.60	11.01	10.10	6.40	5.88	3.67	4.60	2.61	2.13

3.2.2.1 Opaque

The opaque minerals are mainly constituted of iron oxides such as ilmenite, magnetite, hematite, and goethite and mostly found in subrounded, angular and irregular shapes. These minerals were counted and reported as

opaques because it is not possible to identify their individuals without the use of the reflected light. They are found associated with transparent rock-forming minerals. These minerals constituted the greater part of the heavy minerals in all soil samples (Table 3). Their content varies widely from 35.78 to 91.25% of

the total heavy minerals. Also, the frequency distribution of the soil surface layers differs between 59.01 and 87.00% (Figure 7). The lowest content is

recorded in the deepest layer of soil profile 1, meanwhile the deepest layer of soil profile 10 comprehends the highest percentage.

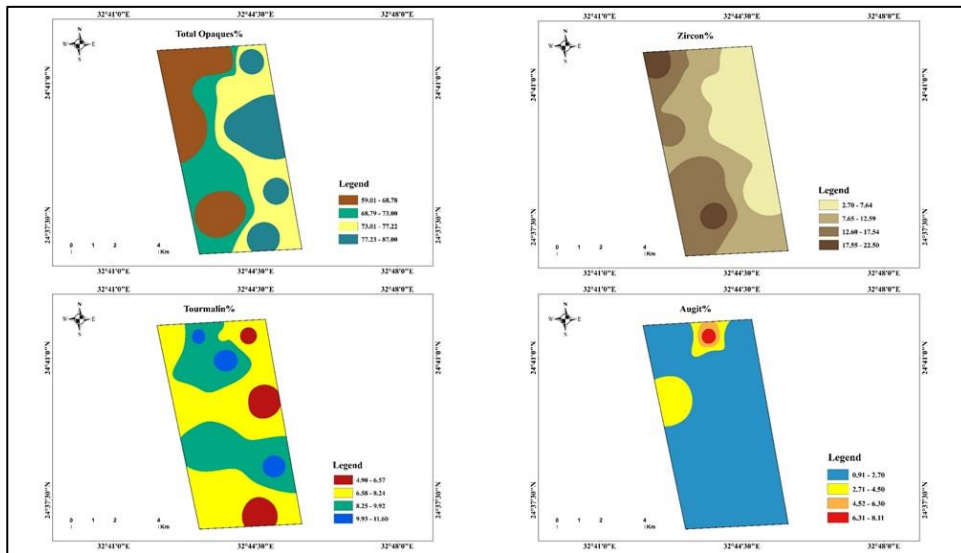


Figure (7): Frequency distribution of opaques, zircon, tourmaline and augite minerals in the soil surface layers of the studied area.

No consistent trends of variations in such minerals could be noted within most soil profile (Figure 8).

3.2.2.2 Zircon

Zircon grains are characterized by their trigonal system, prismatic habit with pyramidal terminations, colorless, very high relief, parallel extinction, strong birefringence, uniaxial positive interference figure and inclusions are

represented by fluid and glass. It shows a maximum frequency of 22.50% of the non-opaque minerals in the surface layer of profile 1 and a minimum frequency of 2.10% in the deepest layer of profile 12 as given in Table (3). Irregular pattern of the frequency distribution in most soil profiles can be observed with depth (Figure 8). Whist the frequency distribution of the soil surface layers differs between 2.70 and 22.50% as illustrated in Figure (7).

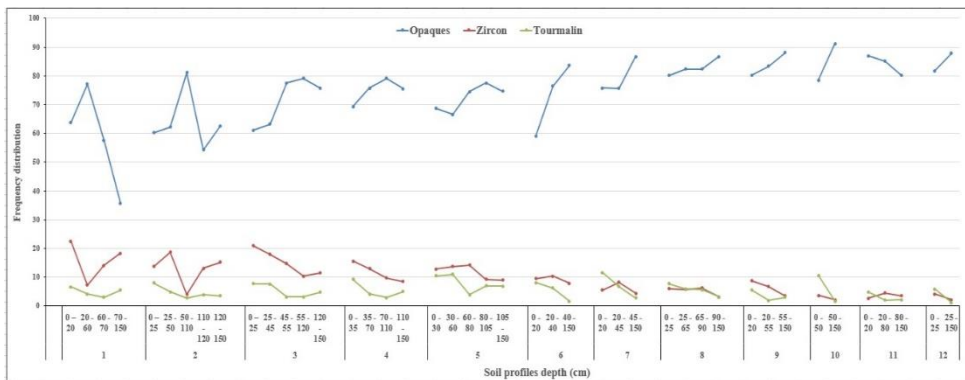


Figure (8): Frequency distribution of opaques, zircon and tourmaline minerals with soil profiles depth of the studied area.

3.2.2.3 Tourmaline

Tourmaline mineral occurs in all estimated samples in significant quantities as its frequency differs among 1.10 to 11.60% (Table 3). Moreover, it recorded in the soil surface layers (4.90 and 11.60%) as shown in Figure (7). The highest percentage is recorded in surface layer of profile 7, whereas the lowest one is found in deepest layer of profile 12. Its distribution with depth shows decrease trend in soil profiles 6, 7, 8, 9, 10 and 12 as given in Figure (8). Tourmaline is characterized by its trigonal system, well-rounded prismatic form, it appears as green to brown grains, strong pleochrism with maximum absorption parallel to the analyzer vibration, negative uniaxial interference figure, parallel extinction and strong birefringence.

3.2.2.4 Pyroxenes

Pyroxene minerals in the studied samples are found in form of augite and enstatite.

3.2.2.4.1 Augite

Augite is detected as prismatic yellowish green, sometimes brown grain, showing no pleochroism with high oblique extinction angle, very high relief, strong birefringence and biaxial positive interference figure. Augite exists in more abundant rather than enstatite where its content differs widely between 0.51 to 11.01%. While the frequency distribution of the soil surface layers varies from 0.91 and 8.11% (Figure 7). The highest percentage of augite mineral characterizes the deepest layer of profile 1 while the lowest one is found in the third layer of profile 3. Most soil profiles exhibit no systematic pattern of the vertical distribution of augite amounts with depth as shown in Figure (9).

3.2.2.4.2 Enstatite

Enstatite is characterized by their grey and greenish prismatic grains with parallel extinction, weak birefringence

and biaxial positive interference figure. Data in Table (3) indicate that, the frequency distribution of enstatite mineral varies between 0.20 and 10.10%, without any distinct trend with depth in most of soil profiles (Figure 9).

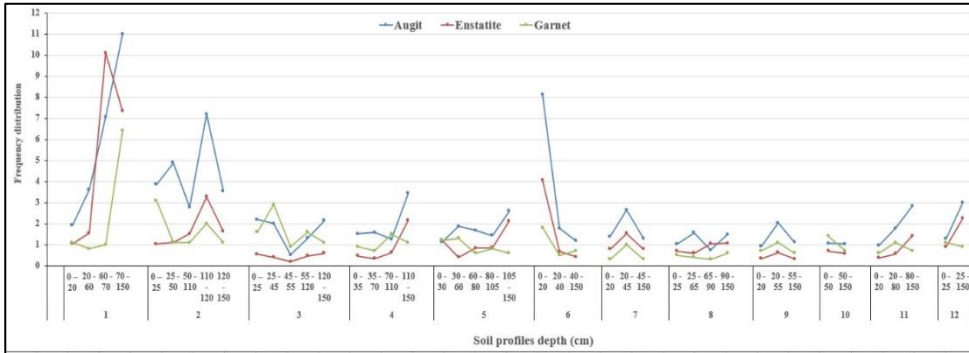


Figure (9): Frequency distribution of augite, enstatite and garnet minerals with soil profiles depth of the studied area.

Where the maximum content is existed in the third layer of profile 1 (gravelly sand). Furthermore, the frequency distribution of the soil surface layers ranges among 0.33 and 4.05% (Figure 10).

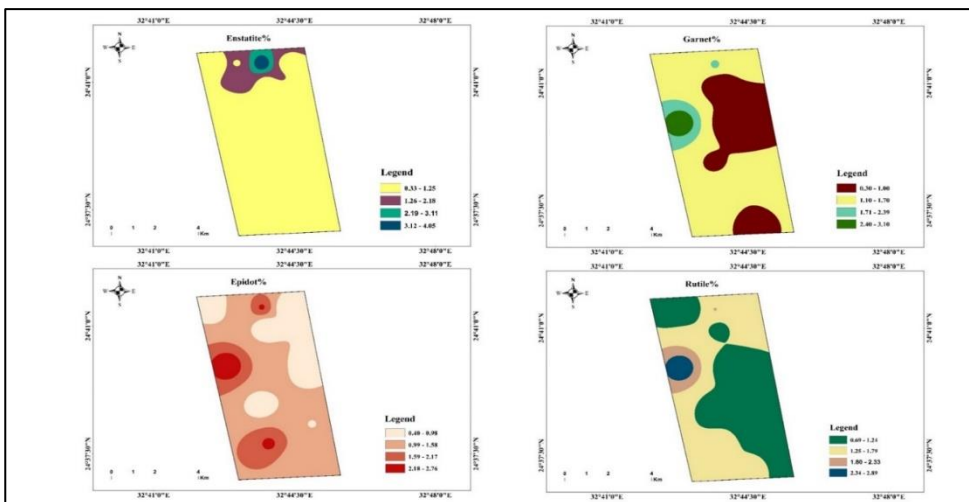


Figure (10): Frequency distribution of enstatite, garnet, epidot and rutile minerals in the soil surface layers of the studied area.

3.2.2.5 Garnet

The metamorphic silicate minerals are represented by garnet that is an alumina-silicate. Garnet is found in a cubic form. The microscopic examination revealed that, the mineral grains are mainly colourless having high relief; no cleavage; rounded and subangular. The content of this mineral varies from 0.30 to 6.40% (Table 3). It shows irregular distribution with depth throughout most of the studied soil profiles (Figure 9). While the frequency distribution of the

soil surface layers ranges among 0.30 and 3.10 % as given in Figure (10).

3.2.2.6 Epidotes

The frequency distribution of epidotes ranges from 0.33% in the deepest layer of profile 12 to 5.88 % in the fourth layer of profile 2 (Table 3). Whilst the frequency distribution of the soil surface layers varies from 0.40 and 2.76 % as illustrated in Figure (10). The distribution of epidotes within soil profiles does not have any specific pattern (Figure 11).

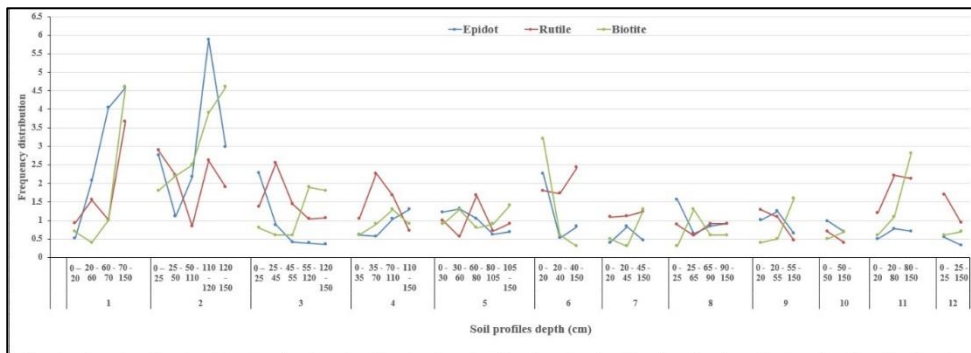


Figure (11): Frequency distribution of epidotes, rutile and biotite minerals with soil profiles depth of the studied area.

They mainly include pistacite and less amounts of zoisite and clinozoisite. Pistacite appears as irregular prismatic, yellowish green grains, giving weak pleochroism, strong birefringence and negative biaxial interference figure. Zoisite and clinozoisite are characterized by prismatic colorless grains with ultra-blue interference tints, but they are different in extinction since the former shows parallel extinction, whereas the latter shows oblique extinction.

3.2.2.7 Rutile

Nonsilicate oxide minerals are mainly represented by rutile. Rutile mineral is detected within all the investigated samples in lower amounts. The mineral amounts are not exceeding 3.67% of the non-opaque minerals without irregular trend with depth in most different layers of soil profiles (Table 3 and Figure 11). The frequency distribution of the soil surface layers in the range of 0.69 to

2.89% (Figure 10). It is characterized by a tetragonal system, a prismatic form with pyramidal termination, often with slightly rounded habit, a reddish brown or a bloody-red color, high relief, distinct pleochrism, straight extinction, extreme birefringence and a positive uniaxial interference figure.

3.2.2.8 Biotite

Biotite is distinguished by its cleavage flakes with jagged edges, brown or

yellow colour, non-pleochroism, strong birefringence, parallel extinction and negative uniaxial interference figure. Data in Table (3) show that biotite is present in all soil samples as little amounts with a maximum percentage of 4.60% in the deepest layer of profile 2. Moreover, the frequency distribution of the soil surface layers differs among 0.30 to 3.20% (Figure 12). No specific pattern of biotite distribution in most studied soil profiles can be observed with depth as given in Figure (11).

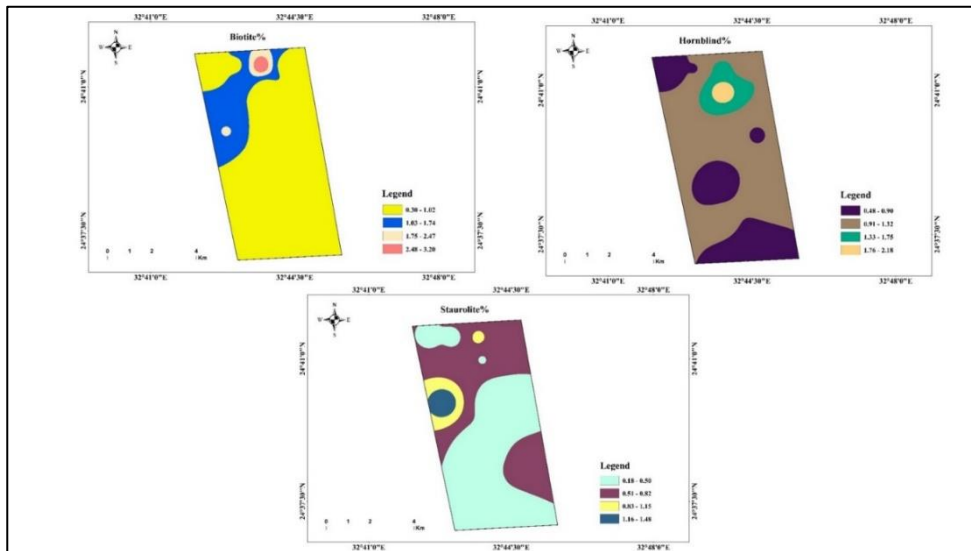


Figure (12): Frequency distribution of biotite, hornblende and staurolite minerals in the soil surface layers of the studied area.

3.2.2.9 Hornblende

Amphiboles minerals in the studied samples are only represented by hornblende. Its grains are characterized by their green elongated platy cleavage

flakes with weak pleochroism, low oblique extinction, moderate birefringence and biaxial negative interference figure. Data in Table 3 show that, hornblende was identified in all the examined samples in amounts ranging

between 0.22 and 2.61% of the non-opaque minerals. Meanwhile the frequency distribution of the soil surface layers varies from 0.48 and 2.18% (Figure 12). Amphiboles minerals show irregular distribution with soil depth in most soil profiles (Figure 13).

3.2.2.10 *Staurolite*

The maximum percentage of staurolite (2.13 %) in the heavy fraction is recorded in the deepest layer of profile 11, without non-consisted trend with depth in most layer of soil profiles (Table 3 and Figure 13).

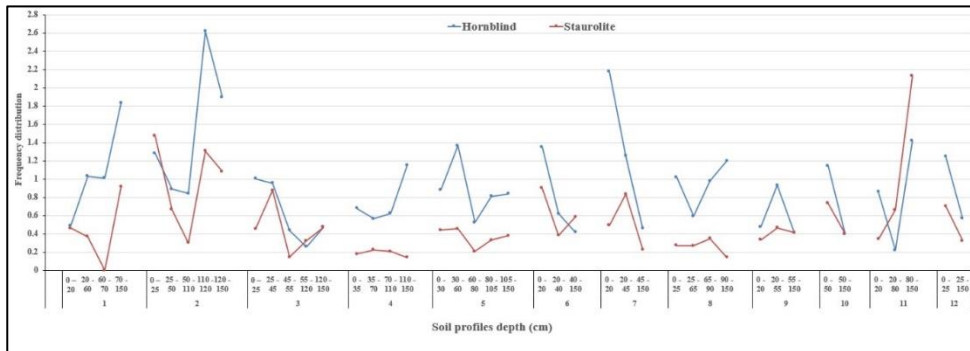


Figure (13): Frequency distribution of hornblende and staurolite minerals with soil profiles depth of the studied area.

However, the frequency distribution of the soil surface layers ranges between 0.18 and 1.48 % (Figure 12). It appears as platy golden yellow to reddish brown grains with moderate pleochroism, moderate birefringence, parallel extinction and positive biaxial interference figure.

3.3 *Index figure*

The index figure values differ among 1.80 and 36.84 %, as shown in Table (4). The varied sources and construction of parent materials and/or depositional processes that contribute to notable variation in the light and heavy minerals composition may be linked to differences in index figures of the studied soils.

3.4 *Soil origin, uniformity and weathering ratios*

Investigation of heavy minerals is counted as standard for evaluating genesis and homogeneity of soil parent material. Cherian *et al.* (2004) and Kasper-Zubillaga *et al.* (2005) recorded some methods such as microscopic analyses to evaluate mode of transportation and consequently genesis of the sediments through the shape and surface features of the grains. The occurrence of quartz in a very high content could reflect the acidic igneous rocks and also feldspars as orthoclase but feldspars as plagioclase indicate the basic igneous origin (Pettijohn, 1975). The occurrence of ferro- and calcium

magnesium- silicate minerals, such as garnet with lesser amounts of monazite, amphiboles and pyroxenes in pronounced amounts and the ultra-stable minerals such as tourmaline, zircon, rutile and staurolite, biotite, apatite and kyanite could indicate igneous and/or metamorphic sources (Milner, 1962).

Table (4): Relative abundance of heavy and light fractions and index figure of very fine sand fraction (0.125-0.063 mm) of representative soil samples of the studied area.

Profile No.	Depth (cm)	Very fine sand Weight (g)	Light fraction		Heavy fraction		Indexfigure (%)
			Weight (g)	(%)	Weight (g)	(%)	
1	0 – 20	2.00	1.88	94.00	0.12	6.00	6.38
	20 - 60	1.13	1.11	98.00	0.02	2.00	1.80
	60 - 70	0.55	0.46	84.00	0.09	16.00	19.57
	70 - 150	0.20	0.18	90.00	0.02	10.00	11.11
2	0 – 25	2.00	1.89	95.00	0.11	6.00	5.82
	25 - 50	2.00	1.91	96.00	0.09	5.00	4.71
	50 - 110	1.44	1.33	92.00	0.11	8.00	8.27
	110 - 120	0.75	0.68	91.00	0.07	9.00	10.29
	120 - 150	0.26	0.19	73.00	0.07	27.00	36.84
3	0 – 25	2.00	1.90	95.00	0.10	5.00	5.26
	25 - 45	2.00	1.83	92.00	0.17	9.00	9.29
	45 - 55	2.00	1.89	95.00	0.11	5.00	5.82
	55 - 120	2.00	1.79	90.00	0.21	11.00	11.73
	120 - 150	2.00	1.90	95.00	0.10	5.00	5.26
4	0 - 35	2.00	1.85	93.00	0.15	8.00	8.11
	35 - 70	2.00	1.89	95.00	0.11	6.00	5.82
	70 - 110	1.81	1.74	96.00	0.07	4.00	4.02
	110 - 150	2.00	1.85	93.00	0.15	8.00	8.11
5	0 - 30	2.00	1.87	94.00	0.13	6.00	6.95
	30 - 60	2.00	1.83	92.00	0.17	9.00	9.29
	60 - 80	2.00	1.94	97.00	0.06	3.00	3.09
	80 - 105	2.00	1.82	91.00	0.18	9.00	9.89
	105 - 150	2.00	1.82	91.00	0.18	9.00	9.89
6	0 - 20	2.00	1.93	97.00	0.07	3.00	3.63
	20 - 40	2.00	1.91	96.00	0.09	4.00	4.71
	40 - 150	2.00	1.90	95.00	0.10	5.00	5.26
7	0 - 20	2.00	1.94	97.00	0.06	3.00	3.09
	20 - 45	2.00	1.94	97.00	0.06	3.00	3.09
	45 - 150	1.70	1.61	95.00	0.09	5.00	5.59
8	0 - 25	2.00	1.92	96.00	0.08	4.00	4.17
	25 - 65	2.00	1.92	96.00	0.08	4.00	4.17
	65 - 90	2.00	1.92	96.00	0.08	4.00	4.17
	90 - 150	2.00	1.91	96.00	0.09	5.00	4.71
9	0 - 20	2.00	1.86	93.00	0.14	7.00	7.53
	20 - 55	2.00	1.87	94.00	0.13	6.00	6.95
	55 - 150	2.00	1.87	94.00	0.13	6.00	6.95
10	0 - 50	2.00	1.95	98.00	0.05	3.00	2.56
	50 - 150	2.00	1.91	96.00	0.09	4.00	4.71
11	0 - 20	2.00	1.78	89.00	0.22	11.00	12.36
	20 - 80	2.00	1.94	97.00	0.06	3.00	3.09
	80 - 150	0.90	0.86	96.00	0.04	4.00	4.65
12	0 - 25	2.00	1.91	96.00	0.09	5.00	4.71
	25 - 150	1.53	1.41	92.00	0.12	8.00	8.51

The presence of opaques, pyroxenes and rutile reflect basic igneous rocks; zircon, apatite represent the acidic igneous rocks; epidotes represent the metamorphic rocks and amphiboles, biotite, tourmaline as well as garnet

represents igneous and/or metamorphic rocks (Nechaev and Ispording, 1993). Data in Table (5) representing the frequency distributions of uniformity ratios of zircon/tourmaline (Z/T), zircon/rutile (Z/R) and zircon / (rutile + tourmaline) (Z/R + T). These findings detect some variations among the layers of the profiles. The vertical distribution of the uniformity ratio values in the investigated soil profiles of the study

area change irregularly depth wise (Figure 14). This emphasizes that these soils are formed from materials of multi-origin and/or heterogeneity nature and they could be considered young from the pedologic point of view. The weathering ratios were calculated for the different layers of each soil profile (Table 5 and Figure 15) that provided a fairly good confirmation for the results obtained from the studied uniformity ratios.

Table (5): Uniformity and weathering ratios of some studied soil profiles.

Profile No.	Depth (cm)	Uniformity ratio			Weathering ratio	
		Zr/R	Zr/T	Zr/R+T	A+P/Zr+T	H/Zr+T
1	0 - 20	24.28	3.41	2.99	0.12	0.02
	20 - 60	4.71	1.78	1.29	0.54	0.09
	60 - 70	13.96	4.70	3.52	1.06	0.06
	70 - 150	4.99	3.33	2.00	0.85	0.08
2	0 - 25	4.74	1.71	1.26	0.28	0.06
	25 - 50	8.42	3.82	2.63	0.29	0.04
	50 - 110	4.75	1.43	1.10	0.75	0.12
	110 - 120	5.01	3.36	2.01	0.77	0.15
	120 - 150	8.01	4.34	2.82	0.38	0.10
3	0 - 25	15.27	2.68	2.28	0.13	0.03
	25 - 45	7.06	2.37	1.77	0.13	0.04
	45 - 55	10.21	4.74	3.24	0.06	0.02
	55 - 120	10.00	3.35	2.51	0.15	0.02
	120 - 150	10.77	2.45	1.99	0.20	0.03
4	0 - 35	15.01	1.70	1.52	0.11	0.03
	35 - 70	5.75	3.17	2.04	0.15	0.03
	70 - 110	5.87	3.38	2.14	0.20	0.05
	110 - 150	11.83	1.70	1.49	0.50	0.09
5	0 - 30	12.87	1.22	1.11	0.14	0.04
	30 - 60	24.60	1.25	1.19	0.15	0.06
	60 - 80	8.47	3.64	2.55	0.17	0.03
	80 - 105	12.86	1.31	1.19	0.19	0.05
	105 - 150	9.85	1.30	1.15	0.35	0.05
6	0 - 20	5.27	1.17	0.96	0.77	0.08
	20 - 40	6.03	1.65	1.30	0.18	0.04
	40 - 150	3.26	4.94	1.96	0.21	0.04
7	0 - 20	5.06	0.47	0.43	0.25	0.13
	20 - 45	7.36	1.22	1.05	0.36	0.08
	45 - 150	3.56	1.57	1.09	0.35	0.06
8	0 - 25	6.78	0.78	0.70	0.20	0.07
	25 - 65	9.59	0.97	0.88	0.24	0.05
	65 - 90	6.92	1.13	0.97	0.23	0.08
	90 - 150	3.51	1.00	0.78	0.58	0.19
9	0 - 20	6.82	1.60	1.30	0.12	0.03
	20 - 55	6.25	3.58	2.28	0.41	0.11
	55 - 150	7.59	1.17	1.01	0.28	0.06
10	0 - 50	5.18	0.34	0.32	0.20	0.08
	50 - 150	5.49	1.29	1.05	0.51	0.10
11	0 - 20	2.25	0.55	0.44	0.28	0.11
	20 - 80	2.03	2.25	1.07	0.39	0.03
	80 - 150	1.65	1.67	0.83	1.01	0.25
12	0 - 25	2.47	0.71	0.55	0.34	0.12
	25 - 150	2.24	1.91	1.03	1.81	0.18

Zr = Zircon, R = Rutile, T = Tourmaline, A = Amphiboles, P = Pyroxines, H = Hornblende.

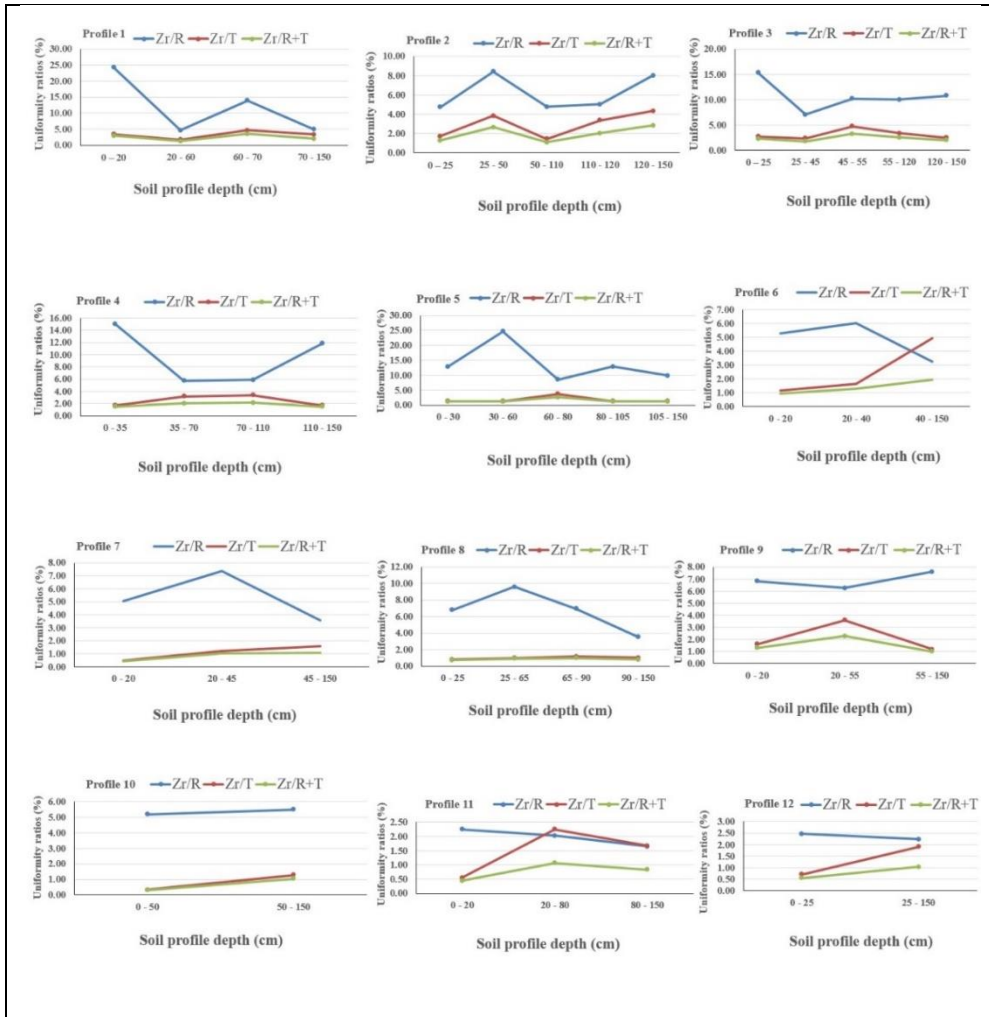


Figure (14): Depth-wise patterns for uniformity ratios of the studied soils.

The results of weathering ratios show that the obtained values are high reflecting the weak effect of weathering processes on these soils under the prevailing arid climate and/or confirm their relatively high content of less stable minerals of pyroxenes and amphiboles. These results also showed that weathering ratios in the surface layer were lower than in the subsurface layer

of the majority of soil profiles that reflect a slight effect of weathering in the surface layer and pronounced amounts of the resistance minerals in these sediments. The variations in uniformity and weathering ratios among the soil profiles and also between the layers in each profile emphasize that these soils are formed from multi-origin and/or due to multi-depositional regimes.

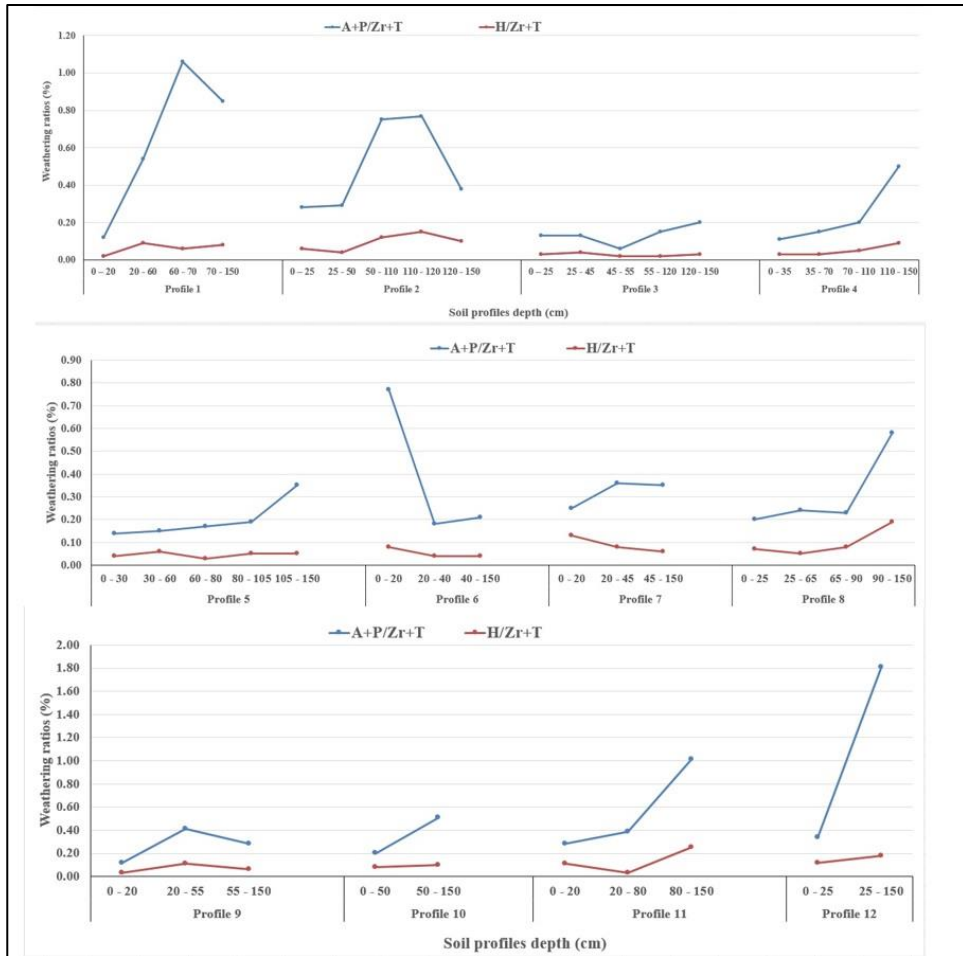


Figure (15): Depth-wise patterns for weathering ratios of the studied soils.

4. Conclusion

The main aims of this paper are to study the mineralogical composition of very fine sand fraction and knowing the origin, uniformity and weathering degree of the soil material in the soils of the investigated area. From the research outputs, it is possible to conclude that the studied soils are recently formed and have low impact of soil forming

processes. The difference and random fluctuation in the distribution of heavy mineral associations in the sand fractions are mainly attributed to variations in nature of provenance, and environment of deposition. The variations in weathering ratios among the soil profiles, as well as between the layers within each profile, emphasize that these soils are formed from multi-origin and/or due to multi-sedimentation regimes.

References

- Abdelhafez, A. A., Metwalley, S. M., and Abbas, H. H. (2020), "Irrigation: Water resources, types and common problems in Egypt", In: Omran E. S., Negm A. (eds), *Technological and Modern Irrigation Environment in Egypt*, Springer Water, Springer International Publishing, Cham, Switzerland, pp. 15–34.
- Ali, M. Y. (2003), *Micropaleontological and stratigraphical analyses of the late cretaceous, early tertiary succession of the southern Nile Valley (Egypt)*, Ph.D. Thesis, Bochum University, Germany, pp. 197.
- Amer, S. A., Elkader, G. A. A. and Dishesh, T. H. M. (2020), "Mineralogical studies on clay and sand fractions as well as homogeneity of soils in south Tushka area, Egypt", *Menoufia Journal of Soil Science*, Vol. 5 No.4, pp.109–131.
- Aref, A. A., El Kady, M. M., Faragallah, M. A. and El-Desoky, A. I. (2021), "Study on genesis and parent material homogeneity of some soils West Manfalut, Assuit, Egypt", *Middle East Journal of Agriculture Research*, Vol. 10 No. 1, pp. 73–91.
- Basheer, A. A. and Mosaad, S. (2018), "Geophysical and hydrogeological evaluation of pliocene aquifer in East Esna, Egypt", *Pure and Applied Geophysics*, Vol. 175 No.6, pp. 2251–2267.
- Brewer, R. (1964), *Fabric and mineral analysis of soils*, John Wiley and Sons Inc., New York, USA.
- Chapman, S. H. and Horn, M. E. (1968), "Parent material uniformity and origin of soils in North-West Arkansas based on Zirconium-Titanium contents", *Soil Science Society of America Journal*, Vol. 32 No. 2, pp. 265–271.
- Cherian, A., Chandrasekar, N. and Rajamanickam, V. (2004), "Light minerals of beach sediments from Southern Tamilnadu, South East coast of India", *Oceanologia*, Vol. 46 No. 2, pp. 233–252.
- Conoco (1987), *A geological maps of Egypt, 1:500000, Luxor sheet*, The Egyptian General Petroleum Corporation/Conoco Coral, Egypt.
- Elwan, A. A. (2021), "Genesis and Uniformity of Some Soils in West El-Minia, Western Desert, Egypt", *Journal of the Advances in Agricultural Researches*, Vol. 26 No. 4, pp. 479–502.
- ESRI (2014), *Arc Map version 10.4.1. user manual*, ESRI, California, New York, USA.
- Farragallah, M. A. and Essa, M. A. (2011), "Mineralogical composition of Khamsin wind dust at Assiut, Egypt", *Assiut University Bulletin for Environmental Researches*, Vol. 14 No. 2, pp.95–108.
- Gavlak, R., Horneck, D. and Miller, R.

- O. (2005), *Soil, plant and water reference methods for the western region*, 3rd Edition, Western Region Extension Publication (WREP-125), Oregon, USA.
- Hammad, M. A. (1968), *Genesis of the soils of the Western Mediterranean Coast of U.A.R.*, Ph.D. Thesis, Faculty of Agriculture, Ain Shams University, Egypt.
- Hewaidy, A. A. and Soliman, S. I. (1993), "Stratigraphy and Paleocology of Gabal El-Borga, South-West KomOmbo, Nile Valley, Egypt", *Egyptian Journal of Geology*, Vol. 37 No. 2, pp. 299–321.
- Kasper-Zubillaga, J. J., Dickinson, W. W. Carranza-Edwards, A. and Hornelas-Orozco, Y. (2005), "Petrography of quartz grains in beach and dune sands of Northland, North Island, New Zealand", *New Zealand Journal of Geology and Geophysics*, Vol. 48, pp. 649–660.
- Keer, P. F. (1959), *Optical Mineralogy*, 3rd edition, Mc Graw- Hill Book Co. Inc., New York, USA.
- Lizzoli, S., Raigemborn, M. S. and Varela, A. N. (2021), "Controls of pedogenesis in a fluvial-eolian succession of Cenomanian age in Northern Patagonia", *Palaeogeography, Palaeoclimatology, Palaeoecology*, Vol. 577, Article ID: 110549.
- Milner, H. B. (1962), *Sedimentary Petrography (Vols. I and II)* George, Allen and Union Ltd., London, England.
- Mosaad, S. and Basheer, A. A. (2020), "Utilizing the geophysical and hydrogeological data for the assessment of the groundwater occurrences in Gallaba Plain, Western Desert, Egypt", *Pure and Applied Geophysics*, Vol. 177 No. 7, pp .3361–3382.
- NASA (2013), *The Thematic Mapper*, Available: <https://landsat.gsfc.nasa.gov>, accessed 1 July 2013.
- Nechaev, V. P. and Isphording, W. C. (1993), "Heavy mineral assemblages of continental margins as indicators of plate-tectonic environments", *Journal of Sedimentary Research*, Vol. 63 No. 6, pp. 1110–1117.
- Pettijohn, F. J. (1975), *Sedimentary Rocks*, Harper and Row Publishers, Inc., New York, USA, 628 pp.
- Poeplau, C. and Kätterer, T. (2017), "Is soil texture a major controlling factor of root: shoot ratio in cereals?", *European Journal of Soil Science*, Vol. 68 No. 6, pp. 964–970.
- Said, R. (1990), *The geology of Egypt*, Balkema Publisher, Rotterdam, Holland, pp. 734.
- Saleh, A. M., Belal, A. B. and Mohamed, E. S. (2015), "Land resources assessment of El-Galaba basin, South Egypt for the potentiality of agriculture expansion using remote sensing and GIS techniques", *The*

- Egyptian Journal of Remote Sensing and Space Science*, Vol. 18 No. 1, pp. 19–30.
- Salman, A. K., Aldulaimy, S. E., Mohammed, H. J. and Abed, Y. M. (2021), "Performance of soil moisture sensors in gypsiferous and salt-affected soils", *Biosystems Engineering*, Vol. 209, pp. 200–209.
- Schoenberger, P. J., Wysocki, D. A. and Benham, E. C. (2012), *Field Book for Describing and Sampling Soils*, Version 3.0, Natural Resources Conservation Service, National Soil Survey Center, Lincoln, Nebraska, USA.
- Siqueira, R. G., Schaefer, C. G. R., Filho, E. I. F., Correa, G. R., Francelino, M. R., Souza, J. J. L. and Rocha, P. A. (2021), "Weathering and pedogenesis of sediments and basaltic rocks on Vega Island, Antarctic Peninsula", *Geoderma*, Vol. 382, Article ID: 114707.
- Sulieman, M. M., Sallam, A. S., Brevik, E. C. and Al-farraj, A. S. (2021), "Early indicators of pedogenesis at Harrat Khaybar volcano, Saudi Arabia", *Geoderma*, Vol. 383, Article ID: 114743.
- Sys, C. (1979), *Land evaluation criteria for irrigation*, Volume 50, Report of an Expert Consultation Held in Rome, Italy.
- Yossif, T. M. H., Abdel-Gaphour, E. A. and Khalifa, M. E. A. (2022), "Assessment of the origin, formation and uniformity of some soils, South of Rood El Farj- El Dabaa Road", *Current Science International*, Vol. 11 No. 2, pp. 224–243.